RSC Advances

RSC Advances

www.rsc.org/advances

ROYAL SOCIETY OF CHEMISTRY

www.rsc.org/advances

Graphical abstract

ARTICLE TYPE

Superparamagnetic sandwich structured silver/halloysite nanotubes /Fe₃O₄ nanocomposites for 4-nitrophenol reduction

Bin Mu, Wenbo Wang, Junping Zhang, and Aiqin Wang*

Superparamagnetic sandwich structured silver/halloysite nanotubes/Fe₃O₄ (Ag/HNTs/Fe₃O₄) nanocomposites were fabricated by selective modification of the lumen of halloysite nanotubes with silver nanorods and the external wall with Fe₃O₄ nanoparticles. The silver nanonods within the lumen of halloysite nanotubes and the uniform Fe₃O₄ shell on the external wall were confirmed by transmission
10 electron microscope. The Ag/HNTs/Fe₃O₄ nanocomposites exhibit excellent catalytic activity and recyclability for the reduction of 4-nitrophenol to 4-aminophenol by NaBH₄. In addition, the nanocomposites show high efficiency in magnetic separation efficiency due to the high saturation magnetization and superparamagnetism. Therefore, the nanocomposites have a great potential application in the catalytic field as recyclable and low-cost catalysts.

15 1. Introduction

The application of nanotubular materials, *e.g.*,carbon nanotubes (CNTs), as catalyst supports has attracted much attention in recent decades due to their unique tubular structure and extremely large surface area.[1-3] The catalyst nanoparticles can be generated
20 within the limited space in the nanotubes. This strategy prevents not only the agglomeration of catalysts, but also the obscission during use compared with those anchored on the surface of supports. However, CNTs are still too expensive to produce on a large scale up to now. Therefore, alternative low-cost nanotubular
25 materials with comparable advantages to CNTs are highly desired.

Halloysite nanotubes (HNTs) are a kind of natural aluminosilicate nanotubes with 1:1 Al:Si ratio and a stoichiometry of Al₂Si₂O₅(OH)₄·nH₂O.[4] HNTs have been acknowledged as a
30 rising star in the area of material science due to their high porosity, abundance in nature, non-toxic and low cost. Many excellent researches have been reported involving their various potential applications, such as loading and controlled release of drugs, nanoreactors, reinforcement of polymers, and catalysis
35 carriers, etc.[5-8] The hollow tubular structure of HNTs is composed of two-layered aluminosilicate, with gibbsite octahedral sheet of aluminol groups (Al-OH) on the internal surface and siloxane groups (Si-O-Si) on the external surface. This difference in the structure results in a negatively charged
40 external surface and a positively charged inner lumen. Therefore, it is feasible to design novel halloysite-based functional materials by selective modification of its lumen and external wall.

In recent years, the modification of HNTs is mainly focused on the external wall including the organic modification with
45 organosilanes and polymers,[9-11] and the deposition of metal and metal oxide nanoparticles.[12,13] This might be attributed to the easy modification of siloxane groups on the external surface of HNTs. The nanotubular structure of HNTs can also provide a confined space for the catalysts and reactions. However, it is rarely
50 reported that metal and metal oxide catalysts are generated within the lumen of HNTs due to the electrostatic repulsion between metal cations and the positively charged inner lumen. Only organophosphate and catechol or dopamine derivatives were used to selectively modify the inner surface of HNTs due to their high
55 affinity toward metal oxide.[14,15] Yan et al. prepared CoFe₂O₄/HNTs magnetic composites via a wet impregnation technique.[16] The magnetic CoFe₂O₄ nanoparticles were successfully encapsulated in the lumen of HNTs. However, the structure of HNTs might have been destroyed in preparing the
60 CoFe₂O₄/HNTs magnetic composites, because the concentrated sulfuric acid can selectively etch alumina inside the nanotubes.[17] Therefore, the magnetic CoFe₂O₄ nanoparticles might be generated within the silica nanotubes instead of HNTs due to the etching of alumina.[18] Lvov et al. synthesized silver nanorods in
65 limited space of the HNTs lumen. The technique required thermal decomposition of silver acetate at 300 °C after being loaded into the lumen under reduced pressure.[19] The pore size of the original HNTs was in the range of 0~150 nm according to the nitrogen adsorption method.[20] It was reported that the pore size of HNTs
70 decreased with increasing temperature, especially the meso- and macropores ranged from 30 nm to 130 nm at the temperature over 300 °C. Therefore, it is difficult to generate metal and metal oxide catalysts in a confined space of the HNTs lumen without damage its structure.

75 Here we described the synthesis, characterization and catalytic activity of superparamagnetic sandwich-structured silver/halloysite nanotubes/Fe₃O₄ (Ag/HNTs/Fe₃O₄) nanocomposites. The Ag/HNTs/Fe₃O₄ nanocomposites were fabricated by selective modification of the lumen of HNTs with

silver nanorods and the external wall with Fe_3O_4 nanoparticles. The nanocomposites were prepared under mild condition in order to keep the structure of HNTs. The reduction of 4-nitrophenol (4-NP) with $NaBH_4$ was chosen as a model reaction to evaluate the catalytic activity of the nanocomposites. Based on the example of the catalytic reduction of 4-NP, it can be confirmed that $Ag/HNTs/Fe_3O_4$ nanocomposites possess enhanced catalytic activity and cycling stability compared with Ag nanoparticles anchored on the external wall of HNTs.

2. Materials and methods

2.1. Materials

HNTs were purchased from Sigma-Aldrich. Silver nitrate ($AgNO_3$) was obtained from Shanghai Chemical Reagent Co. Ltd. Ascorbic acid, L-lysine and other chemicals were purchased from Sinopharm Chemical Reagent Co. Ltd. All the chemicals are of analytical grade and used without further purification. Ultrapure water (resistivity = 18.25 MΩ cm) was used throughout the experiments.

2.2. Generating Ag nanorods within the lumen of HNTs

The introduction of Ag nanorods within the lumen of HNTs was performed according to the following procedure. 1.0 g of HNTs was added into 100 mL of water containing 1.0 g of ascorbic acid under stirring. The suspension was transferred into a vacuum jar after being ultrasonically dispersed for 1 h and evacuated using a vacuum pump for 30 min. The process of air evacuation and cycling back to atmospheric pressure was repeated three times. After being stirring for 2 days at room temperature, the products were washed with H_2O and centrifuged until no ascorbic acid was detected in the supernate. The HNTs loaded with ascorbic acid was re-dispersed into the aqueous solution containing 5 mmol of $AgNO_3$, and then conducted according to the same procedure as the loading ascorbic acid to induce Ag^+ into the lumen of HNTs. The color of the above mixture gradually became gray, indicating Ag^+ was reduced by the ascorbic acid confined within the HNTs lumen. The final product was denoted as Ag/HNTs after being washed with water and dried under vacuum at 40 °C.

As a control experiment, Ag nanoparticles anchored on the external wall of HNTs were also prepared. In typical procedure, 1.0 g of HNTs was ultrasonically dispersed into 100 mL of water containing 5 mmol of $AgNO_3$, and then the loading of Ag^+ was conducted according to the same procedure as the loading of ascorbic acid, as above. The ascorbic acid solution (0.28M, 20 mL) was added dropwise to reduce the Ag^+ after the HNTs loaded with Ag^+ was dispersed into 80 mL aqueous solution under stirring, and the reaction was allowed to proceed for overnight. The ultimate products were washed more than three times with distilled water to discard the excessive ascorbic acid by the centrifugation, and denoted as HNTs/Ag.

2.3. Electrostatic self-assembly of Lys-Fe_3O_4

Firstly, the L-lysine modified Fe_3O_4 nanoparticles (Lys-Fe_3O_4) were prepared via a one-pot coprecipitation method in the presence of L-lysine. The preparation process was similar with our previous reported method except for replacing sodium citrate with L-lysine.[21] The introduction of Lys-Fe_3O_4 nanoparticles was completed by the self-assembly of Lys-Fe_3O_4 on the surface of Ag/HNTs via electrostatic interaction. The addition of Lys-Fe_3O_4 nanoparticles was divided into several times until the saturated adsorption. Then the brownish black products were separated by a magnet and subjected to repeated washing with water. The as-prepared products were ultimately dried under vacuum at 40 °C and denoted as $Ag/HNTs/Fe_3O_4$.

2.4. Catalytic reduction of 4-NP

To study the catalytic activity, 25.0 mg of the $Ag/HNTs/Fe_3O_4$ nanocomposites was dispersed into 50.0 mL of 4-NP solution (5 mM), which is followed by adding 20 mL of fresh $NaBH_4$ solution (0.1 M). The catalytic reduction reaction was carried out at room temperature with continuous stirring. Parts of the mixture were taken out at different time intervals and separated by a magnet for recording the UV-vis absorption spectra. For the next cycle, the $Ag/HNTs/Fe_3O_4$ catalyst was separated from the reaction system by a magnet, washed three times with ethanol and dried at room temperature.

2.5. Characterization

Bruker IFS 66 v/s IR spectrometer (Bruker, Karlsruhe, Germany) was used for the Fourier transform infrared spectroscopy analysis in the range of 400 to 4000 cm^{-1} with a resolution of 4 cm^{-1}. The morphology of the samples was characterized with a JEM-1200 EX/S transmission electron microscope (TEM) (JEOL, Tokyo, Japan). The X-ray diffraction (XRD) analysis was conducted with an X-ray powder diffractometer with Cu anode (PANanalytical Co. X'pert PRO), running at 40 kV and 30 mA. Magnetic properties of samples were detected by vibrating sample magnetometer (Lakeshore 7304). UV-vis absorption spectra were measured at room temperature by using a Lambda 35 UV-vis spectrometer (PerkinElmer, U.S.A.). The chemical compositions of samples were determined using PANalytical's MiniPal 4, a bench-top energy dispersive X-ray fluorescence (XRF) spectrometer (Netherlands), equipped with a 30 kV chromium anode tube, 5 filters, a helium purge facility, a high-resolution Silicon Drift Detector, a spinner and a 12-position removable sample changer. The zeta potentials of samples in deionized water were determined with a MalvernZetasizer Nano system with irradiation from a 633 nm He-Ne laser (ZEN3600).

3. Results and discussion

3.1. Morphology characterization
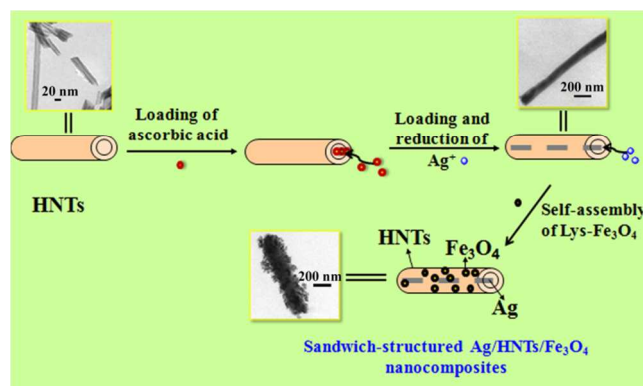
Scheme 1 Synthetic route of the sandwich structured $Ag/HNTs/Fe_3O_4$ nanocomposites

Scheme 1 illustrates the synthetic route of the superparamagnetic

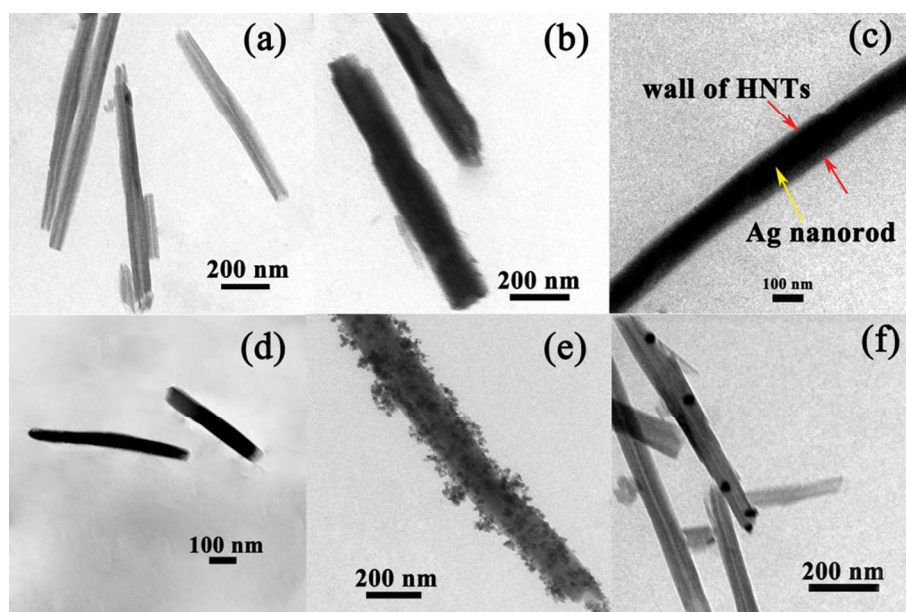**Fig. 1** TEM images of (a) HNTs, (b) and (c) Ag/HNTs, (d) Ag nanorods, (e)Ag/HNTs/Fe$_3$O$_4$ and (e) HNTs/Ag

sandwich structured Ag/HNTs/Fe$_3$O$_4$ nanocomposites. Firstly, the generation of Ag nanorods within the lumen of HNTs is achieved in two steps. It is usually difficult for metal cations to enter into the positively charged lumen of HNTs because of electrostatic repulsion. Therefore, ascorbic acid is firstly introduced into the lumen of HNTs with the help of ultrasonic and reduced pressure. Ascorbic acid is a dibasic acid (pKa$_1$ = 4.25 and pKa$_2$ = 11.79).[22] It can be served as a two-electron reductant with a redox potential of -0.06 V.[22,23] The reduced pressure could effectively evacuate the air from the lumen of HNTs and induce ascorbate anions into the lumen. Then, Ag$^+$ can be reduced in the confined space of the HNTs lumen to format Ag nanorods under vacuum. Subsequently, the magnetic shell is formed on the external wall of Ag/HNTs by the electrostatic self-assembly of the magnetic nanoparticles to construct the sandwich structured Ag/HNTs/Fe$_3$O$_4$ nanocomposites.

The hollow tubular structure and the morphology change of HNTs can be observed with TEM. As shown in Fig. 1a, the TEM image reveals that HNTs are cylindrical-shaped tubes with multilayer walls and open-ended lumen along the nanotubes. It can be clearly seen that there are difference in diameter, wall thickness, and morphology of HNTs. The external and inner diameters of the nanotubes are about 40~80 nm and 15~30 nm, respectively. After selective generation of Ag nanorods within the HNTs lumen, the transparent central channel running longitudinally along the nanotubes becomes less resolved (Fig. 1b). It indicates that the lumen of HNTs has been filled by Ag nanorods with a more deep contrast compared with the walls of HNTs, allowing formation of metal core with insulating aluminosilicate shell, as shown in Fig. 1c. In order to confirm the formation of Ag nanorods, the as-prepared Ag/HNTs nanocomposites were treated with the mixed solution containing HCl and HF to etch HNTs. The TEM image of the Ag nanorods is presented in the Fig. 1d, it can be found that the diameter and the length of the Ag nanorods are around 50~75 nm and 0.5~0.8

μm, respectively. The zeta potential of Ag/HNTs is -28.6 mV, and Lys-Fe$_3$O$_4$ nanoparticles with the protonated amino groups are easily anchored on the external surface of Ag/HNTs via electrostatic interaction. The magnetic nanoparticles are uniformly attached to the surface of Ag/HNTs as shown in Fig. 1e. The zeta potential of Ag/HNTs/Fe$_3$O$_4$ also changed to 30.1 mV, confirming that the magnetic nanoparticles have been successfully deposited on the surface of Ag/HNTs. As can be seen from the TEM image of HNTs/Ag (Fig.1f), only small amount of Ag nanoparticles with a diameter of about 13 nm are attached on the surface of HNTs. This phenomenon is consistent with the reported noble metal/HNTs nanocomposites prepared by a traditional wet impregnation method.[24,25] In other words, the content of noble metal is limited, which might restrict its catalytic activity. Therefore, it is necessary to modify HNTs with silane coupling agent to improve the adsorption site and the binding stability toward noble metals.[26]

3.2 Microstructures and composition analysis

Fig. 2 shows the XRD patterns of HNTs, Ag/HNTs, and Ag/HNTs/Fe$_3$O$_4$ nanocomposite. For the XRD pattern of HNTs, all of the observed diffraction peaks mainly can be indexed to the characteristic peaks of HNTs.[27,28] All XRD patterns exhibit the (001) characteristic diffraction peak at 2θ = 12.1° (d = 7.35 Å), which identifies it as halloysite-7 Å.[29] The diffraction peaks at 20.3° and 24.9° are attributed to the (020) and (002) of HNTs, respectively. It indicates that the structure of HNTs is kept very well in the process of preparing the Ag/HNTs/Fe$_3$O$_4$ nanocomposite. As shown in the XRD pattern of Ag/HNTs, the diffraction peaks at 38.0°, 44.2°, and 64.6° corresponding to (111), (200), and (220) planes of Ag are clearly visible, which confirms the formation of silver crystalline.[30] In the case of Ag/HNTs/Fe$_3$O$_4$, the characteristic diffraction peaks of Fe$_3$O$_4$ at 30.0°, 35.5°, 43.1°, 55.0°, 57.1°, and 62.6° are assigned to the planes of (220), (311), (400), (422), (511) and (440), indicating a

cubic spinel structure.[31] However, the relative intensity of the corresponding diffraction peaks of HNTs decreases after being coated by Fe_3O_4 shell and the diffraction peaks of Ag almost disappear. It might be ascribed to the high content of Fe_3O_4 and
5 smaller concentration of the metallic silver in the Ag/HNTs/Fe_3O_4 nanocomposite, which also could be confirmed by the elemental composition of Ag/HNTs/Fe_3O_4.
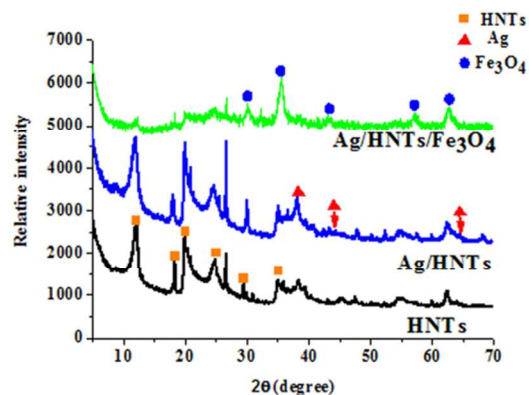

Fig.2 XRD patterns of HNTs, Ag/HNTs, and Ag/HNTs/Fe_3O_4

10 XRF is an analytical technique to determine the elemental composition of various materials.[32] XRF has the advantage of nondestructive, multi-elemental, fast, and cost-effective.[33] The chemical compositions of the original HNTs and Ag/HNTs/Fe_3O_4 nancomposite were determined with XRF (Table 1). The contents
15 of Al, Si, and Fe in HNTs are around 35.2, 50.6, and 4.2, respectively. The Al/Si ratio is 0.696. After being modified with Ag nanorods and magnetic nanoparticles, the contents of Al, Si, Fe, and Ag are about 13.0, 18.3, 56.2 and 8.9, respectively. It can be found that the contents of Al and Si deceased compared with
20 those of HNTs while the Al/Si ratio is almost same as that of HNTs. The decrease in the content of Al and Si is ascribed to the increase in the content of Fe and the presence of Ag. Furthermore, the content of silver in the HNTs/Ag is 0.8%. It is lower than that of Ag/HNTs/Fe_3O_4, which is also consistent with
25 the TEM result.

Table 1 Elemental composition (atomic %) of HNTs, Ag/HNTs/Fe_3O_4 and HNTs/Ag

Elements	Si	Al	Fe	K	Ca	Ag
HNTs	50.6	35.2	4.2	1.4	4.6	—
Ag/HNTs/Fe_3O_4	18.3	13.0	56.2	0.6	0.3	8.9
HNTs/Ag	50.7	36.9	4.6	0.9	0.4	0.8

The FTIR spectrum of HNTs is presented in Fig. 3. The
30 absorption bands at 3690 and 3620 cm^{-1} are ascribed to O-H stretching of the inner-surface hydroxyl groups of Al-O-H, while the band at 914 cm^{-1} is ascribed to O-H deformation of hydroxyl groups.[34] The existence of interlayer or adsorbed water is confirmed by the stretching vibration at 3450 cm^{-1} and the
35 corresponding deformation vibration at 1638 cm^{-1}. The absorption bands at 1083 and 1025 cm^{-1} are ascribed to the in-plane stretching vibration of Si-O, and the band at 751 cm^{-1} is ascribed to the Si-O perpendicular stretching.[35] The bending

vibration of Si-O and stretching vibration of Al-O are presented
40 at 536 cm^{-1} and 462 cm^{-1}, respectively.[36] It can be found the typical absorption band of Fe-O stretching vibration at 580 cm^{-1} from the IR spectrum of Lys-Fe_3O_4.[37] In addition, the absorption bands at 2960 and 2870 cm^{-1} are assigned to the asymmetric and symmetric stretching vibration of C-H, indicating the bonding of
45 L-lysine on the surface of Fe_3O_4 nanoparticles. After being modified with Ag nanorods and Fe_3O_4 nanoparticles, the IR spectrum of Ag/HNTs/Fe_3O_4 is almost the same as that of HNTs, indicating the structure of HNTs is kept very well. In addition, the characteristic absorption band of Fe-O stretching vibration at
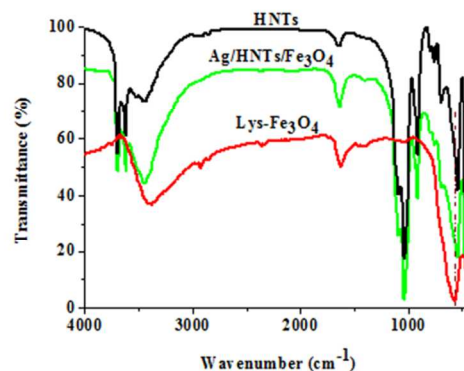50 about 580 cm^{-1} is overlapped with the bending vibration of Si-O.

Fig.3 FTIR spectra of HNTs, Lys-Fe_3O_4 and Ag/HNTs/Fe_3O_4

3.3 Magnetic property
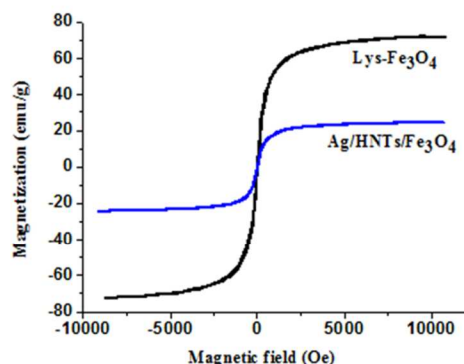
55 **Fig.4** Magnetic hysteresis curves of Lys-Fe_3O_4 and Ag/HNTs/Fe_3O_4

The magnetic properties of Lys-Fe_3O_4 and Ag/HNTs/Fe_3O_4 are investigated by VSM at room temperature. Fig. 4 displays the magnetic hysteresis curves of Lys-Fe_3O_4 and the Ag/HNTs/Fe_3O_4 nanocomposites. Neither remanence nor coercivity is observed,
60 indicating the superparamagnetic property.[38] The saturation magnetization values of Lys-Fe_3O_4 and Ag/HNTs/Fe_3O_4 are 72.53 emu g^{-1} and 24.27 emu g^{-1}, respectively. The saturation magnetization of Ag/HNTs/Fe_3O_4 decreases considerably compared with that of Lys-Fe_3O_4. Such decrease in the saturation
65 magnetization can be attributed to the decrease in the effective
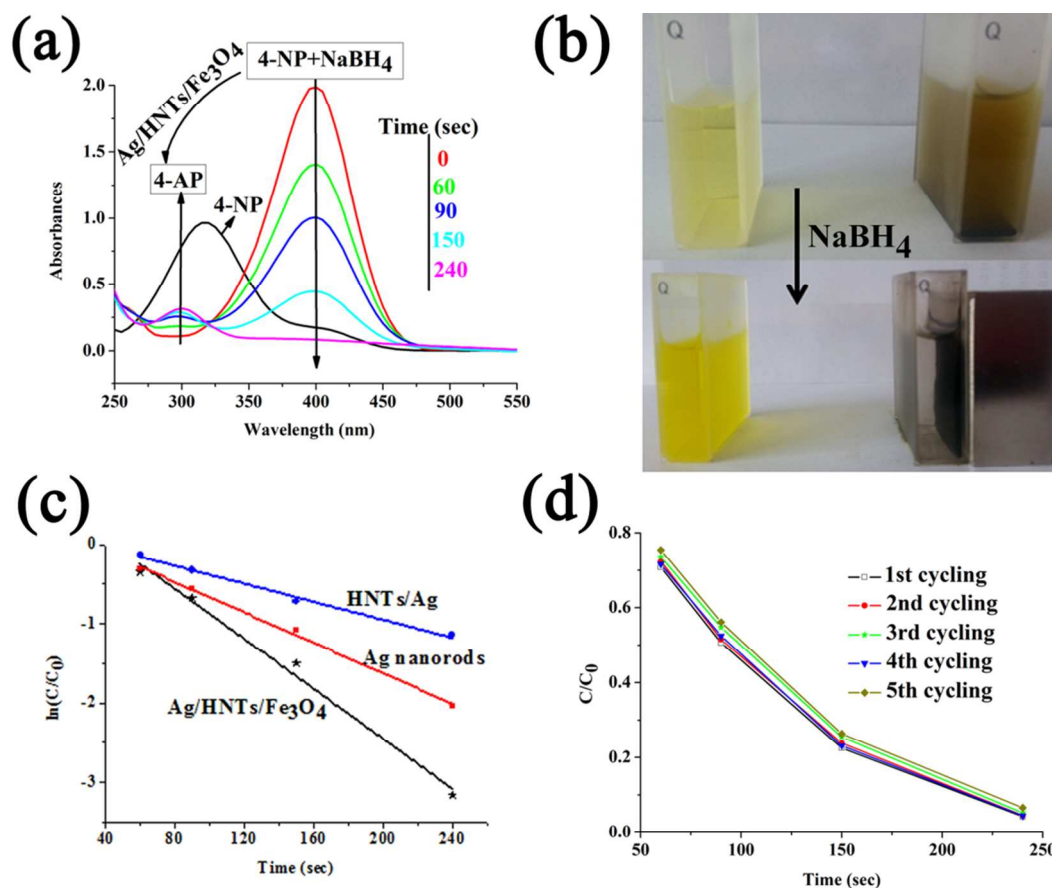
ARTICLE TYPE

Fig.5 (a) Time dependent UV-vis absorption spectra for the catalytic reduction of 4-NP by $NaBH_4$ in the presence of the $Ag/HNTs/Fe_3O_4$ nanocomposite. (b) The solutions composed of 4-NP and the $Ag/HNTs/Fe_3O_4$ nanocomposite before and after adding $NaBH_4$. (c) Linear relationship of $ln(C/C_0)$ as a function of time for the catalytic reduction of 4-NP by the $Ag/HNTs/Fe_3O_4$, HNTs/Ag nanaocomposites and Ag nanorods. (d) Catalytic activity of the $Ag/HNTs/Fe_3O_4$ nanocomposite for 4-NP in five cycles

mass of magnetite due to the existence of HNTs and Ag. The magnetite content also can be calculated to be 34% according to the ratio of the original saturation magnetization of $Lys-Fe_3O_4$ and $Ag/HNTs/Fe_3O_4$. Therefore, the magnetism of the $Ag/HNTs/Fe_3O_4$ nanocomposite is still strong enough to be easily separated using a magnet.

3.4 Catalytic activity and magnetic recycling

The $Ag/HNTs/Fe_3O_4$ nanocomposite with superparamagnetic and catalytic activity has significant potential applications in the area of catalytic reduction and oxidation served as a recyclable catalyst. The reduction of 4-nitrophenol (4-NP) by $NaBH_4$ was chosen as a model reaction to evaluate the performance of the $Ag/HNTs/Fe_3O_4$ nanocomposite, because it can be conveniently monitored by UV-vis absorption spectroscopy and no side reaction occurs in the reduction process of 4-NP. Furthermore, it is also acknowledged as an alternative effective and eco-friendly route to prepare 4-aminophenol (4-AP) by the reduction of 4-NP

in the presence of noble metal-based catalysts.[39]

The aqueous solution of 4-NP has a maximum absorption at 317 nm. However, this peak immediately red shifted to 400 nm after the addition of freshly prepared $NaBH_4$ solution (Fig. 5a). This peak is assigned to the formation of 4-nitrophenolate ions in alkaline condition caused by the addition of $NaBH_4$. Fig. 5a also shows the successive UV-vis spectra of 4-NP in the presence of $NaBH_4$ and $Ag/HNTs/Fe_3O_4$ in aqueous solution. The absorbance at 400 nm gradually decreases, while a new peak at 298 nm appears and increases with the reaction time. The peak at 298 nm can be indexed to the characteristic absorbance peak of 4-AP, which further confirms that 4-NP is reduced to 4-AP. After the catalytic reduction, the peak assigned to the nitro compound at 400 nm disappeared, indicating that the catalytic reduction of 4-NP was completed.
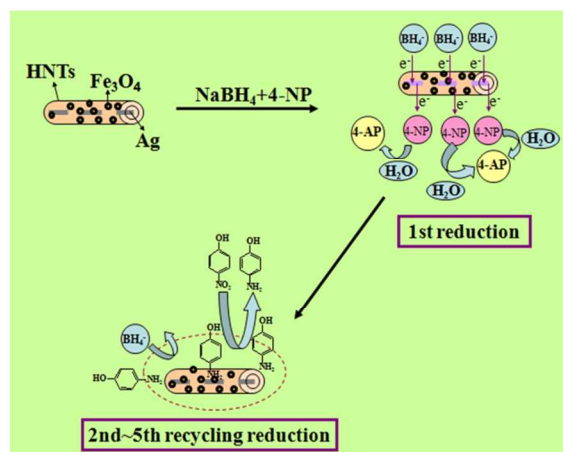
Without the $Ag/HNTs/Fe_3O_4$ nanocomposite, the solution of 4-nitrophenolate ion with a yellow-green color remains unaltered at all with time gone, indicating that the reduction of 4-NP does not

occur (Fig. 5B). However, the reduction of 4-NP by NaBH$_4$ is very rapid in the presence of the Ag/HNTs/Fe$_3$O$_4$ catalyst, which could be visualized with the discoloration of the characteristic yellow-green color of 4-nitrophenolate ion. Furthermore, the
5 Ag/HNTs/Fe$_3$O$_4$ catalyst can rapidly gather on the inwall of cuvette using a magnet (Fig. 5b). This result indicates that the Ag/HNTs/Fe$_3$O$_4$ catalyst with good catalytic performance for the reduction of 4-NP can be easily manipulated by an external magnetic field.

10   The progress of the catalytic reduction of 4-NP can be easily followed by the decrease in the absorbance at λ_{max} of 4-NP with time. The rate of reduction is independent of the concentration of NaBH$_4$ due to the large excess of NaBH$_4$ compared with 4-NP. Therefore, the reaction is considered pseudo-first-order with
15 respect to the concentration of 4-NP. Fig. 5c shows $\ln(C_t/C_0)$ versus reaction time for the reduction of 4-NP over the Ag/HNTs/Fe$_3$O$_4$, HNTs/Ag nanocomposites and Ag nanorods obtained after etching HNTs. It can be seen that $\ln(C_t/C_0)$ versus reaction time presents good linear correlations. Furthermore, the
20 HNTs/Ag catalyst exhibits low catalytic activity compared with Ag/HNTs/Fe$_3$O$_4$ nanocomposites and Ag nanonods, which is attributed to the low content of silver in the HNTs/Ag nanocomposites. Furthermore, the results also indicate that HNTs matrix plays an active role in the catalysis. The enhanced
25 catalytic activity of Ag/HNTs/Fe$_3$O$_4$ nanocomposites may be attributed to the fact that the 4-nitrophenolate ions can be adsorbed onto the aluminosilicate shell and will preconcentrates the 4-nitrophenolate ions around the surface of the metal catalysts.[40] Such adsorption increases the concentration of 4-
30 nitrophenolate ions near to the surface of the metal catalysts and the electron transfer occurs from the electron donor BH$_4^-$ to the 4-nitrophenolate ions. Then, the 4-nitrophenolate ions will be reduced to 4-AP at the surface of the metal catalysts and finally desorbs from the surface, leading to an enhanced catalytic activity
35 towards the reduction of 4-NP. The kinetic reaction rate constants of Ag/HNTs/Fe$_3$O$_4$, HNTs/Ag, and Ag nanorods are 1.58×10^{-2} s^{-1}, 5.7×10^{-3} s^{-1} and 9.6×10^{-3} s^{-1} at room temperature, respectively. Fig. 5d shows that the catalytic reduction of 4-NP using Ag/HNTs/Fe$_3$O$_4$ can be easily recycled and reused by magnetic
40 separation upon five successive cycles of reduction reaction, and the catalytic activity remains constant. It suggested that the aluminosilicate shell can efficiently protect the Ag nanorods during catalytic reaction and improve the durability of precious-metal catalysts.[41]

45   The possible catalytic mechanism can be proposed according to the above experimental results as illustrated in Scheme 2. In the case of the catalytic reduction of 4-NP by noble metal, electron transfer takes place from BH$_4^-$ to 4-NP through adsorption of the reactant molecules on to the catalyst surface.[42,43]
50 BH$_4^-$ as a nucleophile can donate electrons to metal catalysts and 4-nitrophenol as an electrophile can capture electrons from the metal catalysts. Thus, metal catalysts play an important role as electron relays for the reduction of 4-nitrophenol with NaBH$_4$.[44] In the present work, the reactant molecules are firstly adsorbed on
55 the surface of supports, and then diffuse to the active site by the pores of HNTs to form the surface complex. Subsequently, the complex is catalyzed to generate the products, and the products finally desorb from the supports. Furthermore, the amino group

of Ag/HNTs/Fe$_3$O$_4$ can contribute to desorption of the products
60 from the catalyst to keep adsorption sites toward reactant in the next recycling reduction. Thus, the Ag/HNTs/Fe$_3$O$_4$ catalyst exhibits good catalytic activity and stability.

Scheme 2 Proposed mechanism for the catalytic reduction of 4-NP with
65   the Ag/HNTs/Fe$_3$O$_4$ nanocomposite

4. Conclusions

In summary, superparamagnetic sandwich-structured Ag/HNTs/Fe$_3$O$_4$ nanocomposites with good catalytic activity have been successfully fabricated by selective modification of the
70 inner lumen and external wall of HNTs. This is a facile approach to generate metal catalysts in a confined space of the HNTs lumen while keeping the structure of HNTs. The as-prepared Ag/HNTs/Fe$_3$O$_4$ catalyst exhibits excellent catalytic activity and recyclability for the reduction of 4-NP to 4-AP. In addition, the
75 Ag/HNTs/Fe$_3$O$_4$ catalysts could be easily separated due to its magnetism. Therefore, the Ag/HNTs/Fe$_3$O$_4$ nanocomposites have a great potential application as recyclable and low-cost catalysts. Furthermore, it is also beyond all doubt that this technique provides a feasible approach to design the novel HNTs-based
80 functional materials by selective modification the lumen and external wall of HNTs to realize their new application.

Acknowledgement

Notes and references

Center of Eco-materials and Green Chemistry, Lanzhou Institute of Chemical Physics, Chinese Academy of Sciences, Lanzhou 730000, China. Fax: 86 931 8277088; Tel: 86 931 4968118; E-mail:
90 *aqwang@licp.cas.cn*

1 P. Serp and E. Castillejos, ChemCatChem, 2010, **2**, 41-47.
2 J. Wang, Z. P. Dong, J. W. Huang, J. Li, K. Liu, J. Jin, and J. T. Ma, RSC Adv., 2013, **3**, 918-922.
3 X. S. Tan, W. P. Deng, M. Liu, Q. H. Zhang and Y. Wang, Chem.
95   Commun., 2009, 7179-7181.
4 T. F. Bates, F. A. Hildebrand and A. Swineford, Am. Mineral., 1950, **35**, 463-484.
5 L. Fan, J. P. Zhang and A.Q. Wang, *J. Mater. Chem. B*, 2013, **1**, 6261-6270.

6 D. G. Shchukin, G. B. Sukhorukov, R. R. Price and Y. M. Lvov, Small, 2005, **1**, 510-513.

7 M. X. Liu, B. C. Guo, M. L. Du and D. M. Jia, Polym. J., 2008, 40, 1087-1093.

8 D. Papoulis, S. Komarneni, D. Panagiotaras, E. Stathatos, D. Toli, K. C. Christoforidis, M. Fernández-García, H. H. Li, S. Yin, T. Sato and H. Katsuki, Appl. Catal. B: Environ., 2013, **132-133**, 416-422.

9 P. Yuan, P. D. Southon, Z. W. Liu and C. J. Kepert, Nanotechnology, 2012, **23**, 375705.

10 P. Yuan, P. D. Southon, Z. W. Liu, M. E. R. Green, J. M. Hook, S. J. Antill and C. J. Kepert, J. Phys. Chem. C, 2008, **112**, 15742-15751.

11 B. Mu, M. F. Zhao and P. Liu, J. Nanopart. Res., 2008, **10**, 831-838.

12 L. Wang, J. L.Chen, L. Ge, V. Rudolph, and Z. H. Zhu, J. Phys. Chem. C, 2013, **117**, 4141-4151.

13 D. Papoulis, S. Komarneni, D. Panagiotaras, E. Stathatos, K. C. Christoforidis, M. Fernández-García, H. H. Li, Y. Shu, T. Sato and H. Katsuki, Appl. Catal. B: Environ., 2014, **147**, 526-533.

14 W. O. Yah, H. Xu, H. Soejima, W. Ma, Y. Lvov and A. Takahara, J. Am. Chem. Soc., 2012, **134**, 12134-12317.

15 W. O. Yah, A. Takahara and Y. M. Lvov, J. Am. Chem. Soc., 2012, **134**, 1853-1859.

16 J. M. Pan, H. Hang, X. H. Dai, J. D. Dai, P. W. Huo and Y. S. Yan, J. Mater. Chem., 2012, **22**, 17167-17175.

17 E. Abdullayev, A. Joshi, W. B. Wei, Y. F. Zhao and Y. Lvov, ACS Nano, 2012, **6**, 7216-7226.

18 Y. Zhang, L. J. Fu and H. M. Yang, Colloid Surf. A-Physicochem. Eng. Asp., 2012, 414, 115-119.

19 E. Abdullayev, K. Sakakibara, K. Okamoto, W. B. Wei, K. Ariga and Y. Lvov, ACS Appl. Mater. Interfaces, 2011, **3**, 4040-4046.

20 Q. Wang, J. P. Zhang, Y. Zheng, A. Q.Wang, Colloid Surf. B, 2014, **113**, 51-58.

21 B. Mu, P. Liu, Y. Dong, C. Y. Lu and X. L. Wu, J. Polym. Sci., Part A: Polym. Chem., 2010, **48**, 3135-3144.

22 A. T. Stone, K. L. Godtfredsen and B. Deng, Sources and reactivity of reductants encountered in aquatic environments. In: Chemistry of Aquatic Systems: Local and Global Perspectives; G. Bidoglio, W. Stumm, Eds.; Kluwer: Dordrecht, The Netherlands, 1993, pp 337-374.

23 M. B. Davies, D. A. Partridge and J. Austin, Vitamin C: Its Chemistry and Biochemistry; Royal Society of Chemistry: Cambridge, UK. 1991.

24 L. Wang, J. Chen, V. Rudolph and Z. Zhu, Adv. Powder Technol., 2012, **23**, 465-471.

25 L.Wang, J. L. Chen, L. Ge, Z. H. Zhu and V. Rudolph, Energy Fuels, 2011, **25**, 3408-3416.

26 H. Zhu, M. L. Du, M. L. Zou, C. S. Xu and Y. Q. Fu, Dalton Trans., 2012, **41**, 10465-10471.

27 R. J. Wang, G. H. Jiang, Y. W. Ding, Y. Wang, X. K. Sun, X. H. Wang and W. X. Chen, ACS Appl. Mater. Interfaces, 2011, **3**, 4154-4158.

28 Y. Zhang and H. M. Yang, Phys. Chem. Miner., 2012, **39**, 789-795.

29 G. W. Brindley, Order-disorder in the clay mineral structures. In Crystal Structures of Clay Minerals and Their X-ray Identification; G.W. Brindley, G. Brown, Eds.; Mineralogist Society: London, 1980, p 125.

30 B. Mu, Q. Wang and A. Q. Wang, *J. Mater. Chem. A*, 2013, **1**, 7083-7090.

31 M. Zhang, B. L. Cushing and C. J. O'Connor, Nanotechnology, 2008, **19**, 085601.

32 R. Jenkins, R. W. Gould, D. Gedcke, Quantitative X-ray Spectrometry, 2nd Edition, Marcel Dekker Inc., New York, 1995.

33 H. Sitepu, M. G. Kapylova, D. H. Quirt, J. N. Cutler and T. G. Kotzer, Am. Mineral., 2005, **90**, 1740-1747.

34 E. Joussein, S. Petit, J. Churchman, B. Theng, D. Righi and B. Delvaux, Clay Miner., 2005, **40**, 383-426.

35 S. Barrientos-Ramirez, E. V. Ramos-Fernandez, J. Silvestre-Albero, A. Speulveda-Escribano, M. M. Pastor-Blas and A. Gonzalez-Montiel, Microporous Mesoporous Mater., 2009, **120**, 132-140.

36 Y. Deng, G. N. White and J. B. Dixon, J. Colloid Interface Sci., 2002, **250**, 379-393.

37 J. Sangeetha and J. Philip, RSC Adv., 2013, **3**, 8047-8057.

38 J. Y. Park, P. Daksha, G. H. Lee, S. Woo and Y. M. Chang, Nanotechnology, 2008, **19**, 365603.

39 S. Tang, S. Vongehr and X. Meng, J. Phys. Chem. C, 2010, **114**, 977-982.

40 A. Walcarius, Electroanalysis, 1998, **10**, 10 1217-1235.

41 J. Lee, K. Han and D. J. Jang, Appl. Catal. A, 2014, **469**, 380-386.

42 S. Jana, S. K. Ghosh, S. Nath, S. Pande, S. Praharaj, S. Panigrahi, S. Basu, T. Endo and T. Pal, Appl. Catal. A, 2006, **313**, 41-48.

43 P. Veerakumara, M. Velayudhamb, K. L. Lub, S. Rajagopala, Appl. Catal. A, 2012, **439-440**, 197-205.

44 Z. X. Wang, X. B. Chen, M. Chen and L. M. Wu, Langmuir, 2009, 25, 7646-7651.